



[Ru(pipe)(dppb)(bipy)]PF₆: A novel ruthenium complex that effectively inhibits ERK activation and cyclin D1 expression in A549 cells



Guilherme A. Ferreira-Silva^a, Marina M. Ortega^b, Marco A. Banionis^a, Graciana Y. Garavelli^a, Felipe T. Martins^c, Julia S.M. Dias^b, Cláudio Viegas Jr^b, Jaqueline C. de Oliveira^d, Fabio B. do Nascimento^e, Antonio C. Doriguetto^b, Marília I.F. Barbosa^{b,*}, Marisa Ionta^{a,**}

^a Institute of Biomedical Sciences, Federal University of Alfenas, zip code 37130-001, Alfenas, MG, Brazil

^b Institute of Chemistry, Federal University of Alfenas, zip code 37130-001, Alfenas, MG, Brazil

^c Institute of Chemistry, Federal University of Goiás, zip code 740011-970, Goiânia, GO, Brazil

^d Department of Genetics, Federal University of Paraná, zip code 80060-000, Curitiba, PR, Brazil

^e Waters Technologies of Brazil, zip code 06455-020, Barueri, SP, Brazil

ARTICLE INFO

Keywords:

Non-small cell lung cancer
Ruthenium complexes
Antiproliferative activity
Apoptosis
A549 cells

ABSTRACT

Lung cancer is the most frequent type of cancer worldwide. In Brazil, only 14% of the patients diagnosed with lung cancer survived 5 years in the last decades. Although improvements in the therapeutic approach, it is relevant to identify new chemotherapeutic agents. In this framework, ruthenium metal compounds emerge as a promising alternative to platinum-based compounds once they displayed lower cytotoxicity and more selectivity for tumor cells. The present study aimed to evaluate the antitumor potential of innovative ruthenium(II) complex, [Ru(pipe)(dppb)(bipy)]PF₆ (PIPE) on A549 cells, which is derived from non-small cell lung cancer. Results demonstrated that PIPE effectively reduced the viability and proliferation rate of A549 cells. When PIPE was used at 9 μM there was increase in G0/G1 cell population with concomitant reduction in frequency of cells in S-phase, indicating cell cycle arrest in G1/S transition. Antiproliferative activity of PIPE was associated to its ability of reducing cyclin D1 expression and ERK phosphorylation levels. Cytotoxic activity of PIPE on A549 cells was observed when PIPE was used at 18 μM, which was associated to its ability of inducing apoptosis by intrinsic pathway. Taken together, the data demonstrated that PIPE is a promising antitumor agent and further *in vivo* studies should be performed.

1. Introduction

Lung cancer is one of the leading causes of death in the world, and non-small cell lung carcinoma accounts for approximately 80% of all lung cancers (Reck et al., 2013). In Brazil, it was reported in 2016 > 17.000 and 10.000 new cases of lung cancer in men and women, respectively. Smoking represents the main cause of lung cancer, and the available treatments are not very effective once the disease is commonly diagnosed in advanced stage. Platinum-based drugs (cisplatin and its analogues) have been used for lung cancer treatment; however, the serious side effects and tumor resistance have limited their clinical application. In this frame, the ruthenium-based compounds represent an alternative to platinum-based compounds due to their versatile chemistry and low toxicity (Allardyce and Dyson, 2001; Komor and Barton, 2013; Barry and Sadler, 2013). The mechanism by which ruthenium complexes exhibit anticancer effects is

variable (Allardyce and Dyson, 2001; Brabec and Nováková, 2006; Kostova, 2006), and it has been related to the nature of the complexes, the ligands involved, and the presence of uncoordinated sites in the coordination sphere of the metal center (Lima et al., 2014). In addition, the ruthenium compounds are not very toxic when compared to platinum-based compounds, and they have been shown to be quite selective for cancer cells (Allardyce and Dyson, 2001; Bergamo and Sava, 2011; Barry and Sadler, 2013).

Three ruthenium compounds (NAMI-A, KP1019, and NKP-1339, a sodium salt of KP1019) reached clinical trials (Sava et al., 1989; Hartinger et al., 2006; Galanski et al., 2003; Flocke et al., 2016; Ang et al., 2011). NAMI-A interferes with the regulation of cell cycle and the extracellular matrix, preventing tumor metastasis, with a current focus on advanced lung cancer (Antonarakis and Emadi, 2010; Bergamo et al., 2012). KP1019 has cytotoxic activity due to its ability in inducing apoptosis by intrinsic pathway and increasing reactive oxygen species

* Correspondence to: Marília I. F. Barbosa, Institute of Chemistry, Federal University of Alfenas, 700, Gabriel Monteiro da Silva Street, Zip code: 37130-001, Alfenas, MG, Brazil

** Correspondence to: Marisa Ionta, Institute of Biomedical Sciences, Federal University of Alfenas, 700, Gabriel Monteiro da Silva Street, Zip code: 37130-001, Alfenas, MG, Brazil
E-mail addresses: marilia.barbosa@unifal-mg.edu.br (M.I.F. Barbosa), marisa.ionta@unifal-mg.edu.br (M. Ionta).

(ROS) formation (Hartinger et al., 2006). Both compounds are of ruthenium(III) and it is believed that their antitumor activity is dependent on *in vivo* reduction to the more reactive ruthenium(II) species. In this framework, there is an increased interest for compounds of ruthenium more stable in the +2 oxidation state (Huxham et al., 2003; Scolaro et al., 2005).

Piperonylic acid is derived from piperine, obtained by alkaline hydrolysis (Si et al., 2013; Zarai et al., 2013). Piperine is a major pungent alkaloid present in black pepper (*Piper nigrum*) and long pepper (*Piper longum*). Piperine antitumor properties have been described (Sunila and Kuttan, 2004; Bezerra et al., 2006; Lai et al., 2012), although there are no reports in the literature on biological effects of piperonylic acid.

The present study aimed to investigate the effects of ruthenium(II)/piperonylic acid complex [Ru(pipe)(dppb)(bipy)]PF₆, from here on called PIPE, on A549 cells, which is derived from lung non-small cell lung cancer (NSCLC).

2. Materials and methods

2.1. Materials and instrumentation

All the synthesis reactions were carried out in an inert atmosphere of argon. Solvents were purified by standard methods and all chemicals used were of reagent grade or comparable purity (Aldrich). The RuCl₃·xH₂O was purchased from Aldrich as well as the ligands 1,4-bis(diphenylphosphino)butane (dppb), 2,2'-bipyridine (bipy) and piperonylic acid were used as received. The *cis*-[RuCl₂(dppb)(bipy)] precursor complex was prepared according to published procedures (Queiroz et al., 1998).

The infrared spectra were recorded on a FTIR Bomem-Michelson 102 spectrometer, with samples prepared as KBr pellets in the 4000–200 cm⁻¹ region. UV–visible spectra were recorded in CH₂Cl₂ solutions at concentration 1.0 × 10⁻³ M on a Shimadzu spectrophotometer UV-2550 model. All NMR experiments were recorded at 293 K on a Bruker spectrometer AC-300 model operating at 300 MHz. The electrochemical experiments were performed at room temperature in CH₂Cl₂ as solvent with tetrabutylammoniumperchlorate (FlukaPurum), with a BAS-100B/W Bioanalytical Systems Inc. electrochemical analyzer; the working and auxiliary electrodes were stationary Pt foils, a Lugging capillary probe was used and the reference electrode was Ag/AgCl. Conductivity measurements were carried out with a Microanal conductometer B-330 model in acetone as solvent. The microanalysis was performed using a Fisons elemental analyzer EA 1108 model.

2.2. X-ray diffraction

Suitably shaped single crystal of the complex was isolated out from mother solution (methanol, dichloromethane, ethyl ether) and quenched at 150 K on the goniometer of a Bruker-AXS Kappa Duo diffractometer with an APEX II CCD detector. MoK α radiation from an I μ S microsource with multilayer optics was employed. Diffraction images were recorded by φ and ω scans set using APEX2 software. This software was also employed to treat the raw dataset for indexing, integrating, reducing and scaling of the reflections. Next, the crystallographic softwares were used as follows: SIR2004 (Burla et al., 2005) (structure solving), SHELXL-97 (Sheldrick, 2008) (structure refinement), MERCURY (Macrae et al., 2008), and ORTEP-3 (Farrugia, 1997) (structure analysis and representation). The structure was solved through identification of all non-hydrogen atoms in its asymmetric unit directly from the Fourier synthesis of the structure factors after retrieval of their phase using the direct methods. The initial model was refined by full-matrix least squares method on F², adopting free anisotropic and constrained isotropic atomic displacement parameters for non-hydrogen and hydrogen atoms, respectively. In the case of hydrogens, their U_{iso} was set to 1.2U_{eq} of the bonded carbon. Hydrogen coordinates

Table 1
Crystal data and structure refinement results for the complex.

Structural formula	C ₄₆ H ₄₁ F ₆ N ₂ O ₄ P ₃ Ru
Fw (g/mol)	993.79
Cryst syst	Monoclinic
Space group	C2/c
Z/Z'	8/1
T (K)	150 (2)
Unit cell dimensions	a (Å)
	b (Å)
	c (Å)
	β (°)
V (Å ³)	8748 (2)
Calculated density (Mg·m ⁻³)	1.509
Absorption coefficient μ (mm ⁻¹)	0.540
θ range for data collection (°)	1.30–25.44
Index ranges	H
	K
	L
Data collected	29,850
Unique reflections	8032
Unique reflections with $I > 2\sigma(I)$	6243
Symmetry factor (R_{int})	0.0467
Completeness to Θ_{max} (%)	99.2
F (000)	4048
Refined parameters	559
Goodness-of-fit on F ²	1.077
R_1 factor for $I > 2\sigma(I)$	0.0528
wR ₂ factor for all data	0.1276
Largest diff. peak/hole (e·Å ⁻³)	0.963/−0.717
CCDC deposit number	1,062,380

were stereochemically defined and constrained in the refinements, oscillating as that of the bonded carbon to keep idealized bond angles and lengths fixed in 0.95 Å (C_{sp}²—H) or 0.99 Å (C_{sp}³—H in CH₂ groups) (Table 1).

2.3. Synthesis of [Ru(pipe)(dppb)(bipy)]PF₆

The obtained complex was synthesized by reaction of *cis*-[RuCl₂(dppb)(bipy)] (0.132 mmol; 100 mg) with piperonylic acid (0.132 mmol; 22.0 mg), in 10 mL of dichloromethane and 10 mL of ethanol under argon atmosphere for 6 h at room temperature. The ligand was previously deprotonated with triethylamine (0.14 mmol; 0.02 mL) and after 1 h NH₄PF₆ (0.129 mmol; 21.0 mg) was added for the precipitation. The solids were filtered, washed in methanol and water and dried *in vacuo*. Yield: 100 mg (78%). C₄₆H₄₁F₆N₂O₄P₃Ru (Calc): C, 55.6; H, 4.2; N, 2.8. (exptl): C, 55.3; H, 4.1; N, 2.5. ³¹P NMR: δ (ppm) 47.5 (d); 33.8 (d), ²J_{P-P}/Hz = 37.8 Hz. ¹H NMR (300 MHz, CDCl₃), δ (ppm): (aromatic hydrogens of bipy): 8.6 (d, 1H); 8.15 (d, 1H); (overlapped signals, 27H aromatic hydrogens of dppb, bipy and pipe); 5.9 (s, 2H piperonal group); 5.94 (d, 1H) and 5.36 (d, 1H) aromatic hydrogens of pipe); (8H, CH₂ of dppb) 3.00–1.5. ¹³C{¹H} NMR (300 MHz, CDCl₃), δ (ppm): (CH₂ of dppb): 22.2 (s, CH₂), 23.6 (s, CH₂), 26.9 (d, ¹J_{CP} CH₂), 28.3 (d, ¹J_{CP} CH₂), 105.5 (s, CH₂ of piperonal group), 106.6 (s, CH pipe), 108.5 (s, CH pipe), 117.9 (s, CH pipe), 122.9 (s, pipe), 123.7 (s, pipe), (CH of dppb and bipy): 124.0 (d), 125.5 (d), 127.0–136.0 (m, C-Ph), 141.5, 148.1, 148.9, 149.3, 155.9, 159.5, 183.4 (s, pipe). Conductivity (Acetone): 95.4 Ω^{-1} ·cm²·mol⁻¹, T = 298 K.

2.4. Cell lines and treatment schedule

A549 (derived from lung cancer) and CCD-1059Sk (normal fibroblast derived from human skin) used in this study, were purchased from Rio de Janeiro Cell Bank. The cell cultures were maintained in DMEM (Dulbecco's Modified Eagle's Medium, Sigma, CA, USA) supplemented with 10% fetal bovine serum (Vitrocell, Campinas, Brazil). Cells were grown in a humidified atmosphere of 95% air and 5% CO₂ at 37 °C. Ruthenium complexes were solubilized in DMSO immediately before

treatment. After attachment (24 h), the cells were treated for 24 h or 48 h according to the experimental approach.

2.5. Cell viability analysis

2.5.1. Colorimetric assay

Cell viability was measured by MTS (dimethylthiazol carboxymethoxyphenyl sulfophenyl tetrazolium) assay using CellTiter 96® Aqueous Non-Radiative Cell Proliferation assay (Promega) according to the manufacturer's instructions. Formazan, the reduced form of tetrazolium, absorbs light at 490 nm and viable cells rate is directly proportional to the amount of produced formazan by dehydrogenase enzymes. Cells were seeded at a density of 5×10^3 cells/well (A549) or 1×10^4 cells/well (CCD-1059Sk) into a 96-well plate. Ruthenium complex was used in different concentrations (0–20 μM) for 24 h or 48 h. Free piperonylic acid and the precursor $[\text{RuCl}_2(\text{dppb})(\text{bipy})]$ were used in a concentration ranging from 0 to 100 μM . Experiments were conducted in triplicate. Data are presented as the mean \pm standard deviation (SD) of three independent experiments. The IC_{50} value was determined from non-linear regression using GraphPad Prism® (GraphPad Software, Inc., San Diego, CA, USA).

2.5.2. Trypan blue exclusion test

Cells were seeded into 35 mm plates at a density of 2×10^5 , and treatment was performed at 9 or 18 μM (PIPE). Cells were harvested with trypsin/EDTA and trypan blue solution (0.4%) was added to cellular suspension (1:1). Subsequently, cells were counted using hemocytometer chamber and light microscope. Non-viable (blue stained) and viable cells (unstained) were quantified from three independent experiments. The results are presented as mean \pm SD.

2.6. Cell cycle analysis

Cell cycle analysis was performed according to Pereira et al. (2016). Briefly, cells were treated with ruthenium complexes for 24 h or 48 h at 9 or 18 μM (PIPE). Cells were fixed with 75% ethanol at 4 °C overnight, rinsed twice with cold phosphate-buffered saline (PBS). Afterwards, cells were homogenized in dye solution [PBS containing 30 $\mu\text{g}\cdot\text{mL}^{-1}$ propidium iodide (PI) and 3 $\text{mg}\cdot\text{mL}^{-1}$ RNAase]. DNA was quantified 1 h after staining. The analysis was performed by flow cytometry (Guava easyCyte 8HT, Hayward, CA, USA). Results are presented as mean \pm SD of three independent experiments.

2.7. Clonogenic assay

Clonogenic assay was performed according to Franken et al. (2006). Briefly, 500 cells were seeded into 35 mm plates. Cells were treated for 24 h and recovered in a drug-free medium for subsequent 15 days. Afterwards, the colonies were fixed and stained with Crystal Violet. Only colonies with > 50 cells were counted by direct visual inspection with a stereomicroscope at 20 \times magnification. Assays were performed in triplicate and data were presented as mean \pm SD of three independent experiments.

2.8. Cytoskeleton elements analysis

Cells were seeded on coverslips and fixed with 3.7% formaldehyde for 30 min. For α -tubulin immunolabelling, cells were permeabilized with Triton X-100 (0.5%) for 10 min. After blocking with 1% BSA, primary antibody (1:100, Sigma Aldrich) was incubated overnight. On next day, secondary anti-mouse IgG-TRITC antibody (1:100, Sigma Aldrich) was added to the sample and incubated for 2 h. Following, phalloidin-FITC (Sigma Aldrich) incubation (1 h) was performed for actin labeling. Nuclei were stained with DAPI and coverslips were mounted on microscope slides using Vecta-Shield (Vector Laboratories). All washes were done with PBS. Analyses were performed using a

fluorescence microscope (Nikon).

2.9. Mitotic index

Mitotic cells were counted from fluorescent cytological preparations containing DAPI stained nuclei; it was counted 1000 cells per sample. Data are shown as mean \pm SD of three independent experiments.

2.10. Immunoblot

Cells were homogenized in RIPA lysis buffer (150 mM NaCl, 1.0% Nonidet P-40, 0.5% deoxycholate, 0.1% SDS and 50 mM Tris pH 8.0) containing both protease and phosphatase inhibitors (Sigma). Lysates were centrifuged (10,000 $\times g$) for 10 min at 4 °C. Supernatants were recovered, total proteins were quantified (BCA kit, Pierce Biotechnology Inc., Rockford, IL, USA) and resuspended in Laemmli sample buffer containing 62.5 mM Tris-HCl pH 6.8, 2% SDS, 10% glycerol, 5% 2-mercaptoethanol and 0.001% bromophenol blue. An aliquot of 50 μg protein was separated by SDS-PAGE (12%) and transferred (100 V, 250 mA for 2 h) on to a PVDF membrane (Amersham Bioscience), blocked for 1 h at 4 °C with blocking solution [5% non-fat milk in Tris-buffered saline (TBS) + 0.1% (v/v) Tween-20] to prevent nonspecific protein binding. The membrane was probed with primary antibodies: (Tyr 204) phosphorylated ERK antibody (Santa-Cruz - 1:50), ERK 1 (Santa-Cruz - 1:1000), Cyclin D1 (Sigma - 1: 200) and α -tubulin (Sigma - 1:1000) overnight at 4 °C. After washing with TBS-tween (0.1%), the membrane was incubated with a secondary antibody (anti-rabbit peroxidase conjugated) for 2 h at room temperature. Immunoreactive bands were visualized with the ECL Western Blotting Detection Kit (Amersham Pharmacia). A reprobing protocol was followed for detecting immunoreactive bands for different antibodies. Results were obtained from three independent experiments. The quantification of immunoreactive bands was performed using a public program (Image J).

2.11. Apoptosis detection by Annexin V/7-AAD

Kit Guava Nexin® (Merk Millipore, Massachusetts, EUA) was used according to manufacturer's instructions. Briefly, cells were collected by enzymatic digestion (Trypsin/EDTA, Sigma), centrifuged at 1000 rpm for 5 min at 4 °C, washed with ice-cold PBS, and then 2×10^4 cells were resuspended in 100 μL of DMEM. In the next step, it was added 100 μL of mix solution containing buffered Annexin V-PE and 7-AAD. The samples were read after 20 min of incubation at room temperature in a dark chamber. The analysis was performed by flow cytometry using GuavaSoft 2.7 software. The experiments were conducted in triplicate and repeated twice. Data are presented as mean \pm SD.

2.12. Mitochondrial membrane potential ($\Delta\psi\text{m}$) analysis by JC-1 fluorescence

Cellular mitochondrial dysfunction can be observed by the loss of the mitochondrial membrane potential, which can be indirectly measured by fluorescence probe JC-1. For this purpose, Guava MitoPotential Kit (Merck/millipore) was used according to manufacturer's instructions. JC-1 is a mitochondrial dye (5,5',6,6'-tetrachloro-1,1,3,3'-tetraethylbenzimidazolylcarbocyanine chloride), that stains mitochondria in living cells in a membrane potential-dependent fashion. The JC-1 monomer is in equilibrium with J-aggregates which binds to the mitochondrial membrane. The monomer JC-1 fluoresces green ($\lambda = 527$ nm), while the J-aggregates fluoresce red ($\lambda = 590$ nm). Therefore, cells with normal mitochondrial membrane potential fluoresce orange. Mitochondria depolarization results in a decrease of the red component and, consequently, green fluorescence. In summary, cells were trypsinized and washed twice with PBS; after that, the cells were labelled with the fluorescent dye JC-1/7-AAD for

30 min at 37 °C. The analysis was performed by flow cytometry using GuavaSoft 2.7 software. The data are shown as mean \pm SD from three independent experiments.

2.13. Cleaved caspase-3 detection

Cells were seeded on coverslips and fixed with 3.7% formaldehyde for 30 min. Cells were permeabilized with Triton X-100 (0.5%) for 10 min. After blocking with 1% BSA, cleaved caspase 3 antibody (1:100, Sigma Aldrich) was incubated overnight at 4 °C. On the next day, secondary anti-rabbit IgG-TRITC antibody (1:100, Sigma Aldrich) was added to the sample and incubated for 2 h. Nuclei were stained with DAPI and coverslips were mounted on microscope slides using Vecta-Shield (Vector Laboratories). All washes were done with PBS. Analyses were performed using a confocal microscope (Nikon).

2.14. Statistical analysis

The results were tested for significance using one-way analysis of variance (ANOVA) followed by a Tukey's post-test using GraphPad Prism®. The values were expressed as mean \pm SD.

3. Results

3.1. Synthesis of the complexes

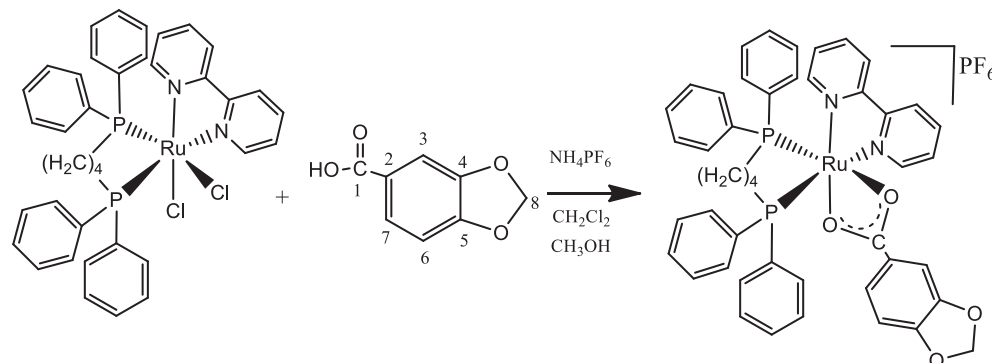
The chemical reactivity of the piperonylic acid ligand with the precursor *cis*-[RuCl₂(dppb)(bipy)] allowed us to synthesize the [Ru(pipe)(dppb)(bipy)]PF₆ complex containing three chelated ligands, in mild conditions by simple chlorides exchange (see Scheme 1).

3.2. Structural studies

The X-ray study confirms the structure proposed for the complex [Ru(pipe)(dppb)(bipy)]PF₆ (Fig. 1) which presents one piperonylic acid, one 2,2'-bipyridine and one 1,4-bis(diphenylphosphino)butane ligands, forming distorted octahedral geometries around metal center as represented by the bonds and angles measurements in the Table 2.

The complex is crystallized in the monoclinic crystal system, with space group C2/c. It is observed that the trans Ru–O bond to the phosphorus atom of the 1,4-bis(diphenylphosphino)butane is longer than the trans Ru–O bond to the nitrogen atom of the 2,2'-bipyridine, confirming the preference of the withdrawal of this chlorine, since this bond is weaker due to strong Ru–P trans interaction to it.

Similarly, when comparing the Ru1-N1 (2.086(4) Å) and Ru1-N2 (2.059(3) Å) bond lengths, the highest binding length for Ru1-N1 is promoted by the competitive effect, since N1 is trans to the phosphorus atom of biphosphine.



Scheme 1. Synthetic route for the preparation of ruthenium complex.

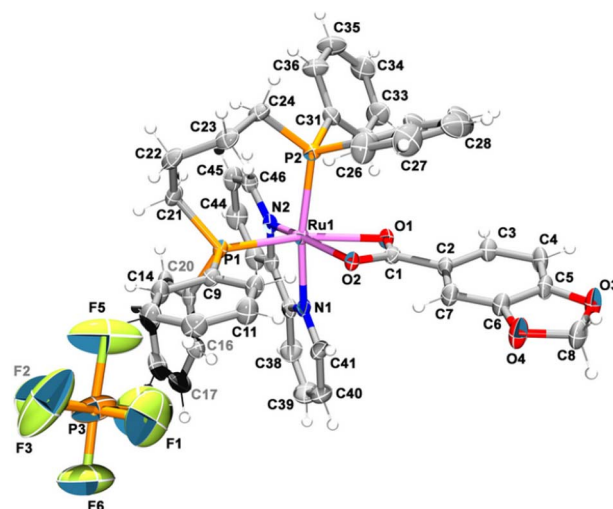


Fig. 1. X-ray structure for [Ru(pipe)(dppb)(bipy)]PF₆, showing atoms labeling and 30% of probability ellipsoids.

Table 2
Bond angles (°) and bond lengths (Å) of Ru(II) complex with e.s.d. in parentheses.

Atoms	Bond angles (°)	Atoms	Bond lengths (Å)
Ru1-N1	2.086 (4)	Ru1-N1	2.086 (4)
Ru1-N2	2.059 (3)	Ru1-N2	2.059 (3)
Ru1-O1	2.245 (3)	Ru1-O1	2.245 (3)
Ru1-O2	2.115 (3)	Ru1-O2	2.115 (3)
Ru1-P1	2.2723 (12)	Ru1-P1	2.2723 (12)
Ru1-P2	2.3079 (12)	Ru1-P2	2.3079 (12)
< N1-Ru1-N2	78.76 (14)	< N1-Ru1-N2	78.76 (14)
< N1-Ru1-O1	83.95 (12)	< N1-Ru1-O1	83.95 (12)
< N1-Ru1-O2	90.36 (13)	< N1-Ru1-O2	90.36 (13)
< N1-Ru1-P1	92.29 (10)	< N1-Ru1-P1	92.29 (10)
< N1-Ru1-P2	168.53 (10)	< N1-Ru1-P2	168.53 (10)
< N2-Ru1-O1	106.59 (12)	< N2-Ru1-O1	106.59 (12)
< N2-Ru1-O2	163.72 (12)	< N2-Ru1-O2	163.72 (12)
< N2-Ru1-P1	88.37 (10)	< N2-Ru1-P1	88.37 (10)
< N2-Ru1-P2	97.59 (11)	< N2-Ru1-P2	97.59 (11)
< O1-Ru1-O2	59.76 (10)	< O1-Ru1-O2	59.76 (10)
< O1-Ru1-P1	163.44 (8)	< O1-Ru1-P1	163.44 (8)
< O1-Ru1-P2	86.74 (8)	< O1-Ru1-P2	86.74 (8)
< O2-Ru1-P1	104.27 (8)	< O2-Ru1-P1	104.27 (8)
< O2-Ru1-P2	90.72 (8)	< O2-Ru1-P2	90.72 (8)
< P1-Ru1-P2	98.50 (4)	< P1-Ru1-P2	98.50 (4)

3.3. Characterization of the compound

The complex [Ru(pipe)(dppb)(bipy)]PF₆ was isolated in acceptable purity, obtained in excellent yield and characterized by elemental analysis (see experimental section), ³¹P{¹H}, ¹³C{¹H} and ¹H NMR spectroscopy, UV–vis, IR, molar conductance and cyclic voltammetry.

$^{31}\text{P}\{^1\text{H}\}$ NMR spectra in CH_2Cl_2 revealed doublets for the compound at 47.5 (d); 33.8 (d) ($^2J_{\text{P-P}} = 37.8$ Hz), which is due to the magnetically different phosphorus atoms, as expected (Fig. S1). Signals at -144 ppm corresponding to the phosphorus atoms of the PF_6^- counter ion were observed. Additionally, in the ^1H NMR spectrum of the free piperonylic acid ligand, a signal corresponding to a singlet of the O–H group proton is observed in 11.0 ppm. This signal is not observed in the spectra of the complex (Fig. S2), indicating the deprotonation of hydroxyl group after its coordination to the metal. Additionally, the ^1H NMR spectra of complex showed the characteristic deshielded signal at 9–8 ppm, corresponding to the ortho hydrogen atoms of the bipy ligand. Other aromatic hydrogen atoms resonances are in the range 6.28–7.94 ppm, which are attributed to the protons present aromatic phosphine, piperonylic acid and bipy. Additionally, a singlet at 5.9 ppm assigned to the CH_2 group of piperonylic ligand was observed. The ^{13}C NMR spectrum of the complex shows that the chemical shift of the carboxylate carbon (C1 – 183.4 ppm) shifts to a lower field region indicating participation of the carboxyl (COO) group in coordination to ruthenium atom. Aromatic carbon atoms of bipy, phosphine and piperonylic acid were also identified in the range 162–100 ppm. The complex present signals at around 20–30 ppm assigned to carbon atoms of the CH_2 groups of the dppb ligand (Barbosa et al., 2015; Lima et al., 2014) (Fig. S3).

In the cyclic voltammogram a quasi-reversible process in 1340 mV that correspond to the redox pair Ru(II)/Ru(III) was observed (Fig. S4). The difference observed between them with precursor may be due to the different stereochemistry found for them. The E1/2 value found for the complex was considerably more anodic than that observed for precursor $[\text{RuCl}_2(\text{bipy})(\text{dppb})]$ (Queiroz et al., 1998), indicating that the ruthenium center is more stable after coordination of piperonylic acid compared with the precursor.

The infrared spectra (IR) of complex show the typical asymmetric $\nu_{\text{as}}(\text{COO}^-)$ and symmetric $\nu_{\text{s}}(\text{COO}^-)$ carboxylate stretching frequencies at 1682 and 1257 cm^{-1} . Free ligand present asymmetric $\nu_{\text{as}}(\text{COO}^-)$ and symmetric $\nu_{\text{s}}(\text{COO}^-)$ carboxylate stretching frequencies at 1674 and 1306 cm^{-1} . The $\Delta\nu$ value of 425 cm^{-1} for complex is indicative of a η^2 binding mode of the carboxylate group. Free ligand presented $\Delta\nu$ value of 368 cm^{-1} (Queiroz et al., 1998; Barbosa et al., 2015; Lima et al., 2014). The characteristic P–F stretch of the PF_6^- counter ion was seen at 837 cm^{-1} (Fig. S5). Most of the vibrational modes observed were characteristic of the dppb and bipy ligands occurring practically at same frequencies observed for the precursor $\text{cis-}[\text{RuCl}_2(\text{dppb})(\text{bipy})]$. The electronic spectra show three bands in the UV region, assigned as intra-ligand transitions by means of comparison with the free ligands (dppb and pip). One band observed in the visible region results from a metal-to-ligand charge transfer transition, probably involving both diimine and piperonylic ligand (Queiroz et al., 1998; Barbosa et al., 2015; Lima et al., 2014) (Fig. S6).

3.4. Morphology, cell viability and proliferation behavior

PIPE reduced drastically A549 cells viability (Fig. 2A) after 24 h and 48 h of treatment. The IC_{50} values found are shown in Table 3. Cisplatin was used as positive control and we verified that PIPE was potentially more effective than cisplatin in reducing A549 cells viability. Cell cultures were also treated with free piperonylic acid and the precursor $[\text{RuCl}_2(\text{dppb})(\text{bipy})]$, however these compounds did not cause reduction in A549 cells viability of and, therefore, the IC_{50} values were not determined. We verified cytotoxic prolife of PIPE on normal cells (CCD-1059Sk) after 48 h of treatment. The IC_{50} value found was 12.43 ± 0.37 μM , approximately 4-fold higher to that found for PIPE on A549 cells in the same experimental condition.

In the next step, we could verify that reduction in cell viability, previously detected by MTS assay, was due to the ability of PIPE in inhibiting cell proliferation and inducing cell death, however these effects were concentration-dependent. According to data obtained by

trypan blue exclusion test, viable cells frequency was significantly reduced (24 h, 25%; 48 h, 60%; and 72 h, 80%) when PIPE was used at 9 μM , despite no significant difference in frequency of dead cells in the treated cultures in comparison to control samples (Figs. 2B and 3A). When PIPE was used at 18 μM , we observed reduction in percentage of viable cells (24 h, 68%; 48 h, 91%; and 72 h, 96%), but we detected a significant increase in dead cells frequency (approximately 50%) in the treated cultures when compared to controls (Figs. 2B and 3A). Thus, PIPE at 18 μM displayed cytotoxic activity on A549 cells.

We performed cell morphology analysis and verified that treatment with PIPE at 9 μM seems to have slight alteration on the morphological aspect of A549 cells; on the other hand, PIPE at 18 μM induced drastic alteration once cells became rounded and less adhered to the substratum (Fig. 2C, upper panel). Cytoskeleton analysis (F-actin and microtubule) allowed us to evidence long microtubule distributed in cytoplasm of the cells treated with PIPE at 9 μM , by contrast to microtubule network evidenced on control cells, suggesting a possible interference of PIPE on dynamic instability of microtubules. Microfilaments distribution also seems to have been altered by treatment once fewer fibers could be observed in the cytoplasm of treated cells, mainly in the cortex region, when compared to control cells that displayed high concentration of actin filaments in the cortex as well as actin stress distributed in the cytoplasm (Fig. 2C, lower panel). The treatment with PIPE at 18 μM caused drastic disturbance in both microtubule and actin filaments network, and this finding could be just related to cytotoxic activity of PIPE when used at this concentration.

We used different methodological approaches to evidence the influence of PIPE on proliferative behavior of A549 cells. Cell viability was assessed again by trypan blue exclusion test at 24 h, 48 h and 72 h; and, in fact, we observed a significant reduction in viable cells number when compared to control cultures (Fig. 3A). Then we observed by flow cytometry that the treatment altered cell cycle progression. There was significant increase in G0/G1 population with concomitant decrease in S-phase and G2/M populations in cultures treated with PIPE at 9 μM . However, when PIPE was used at 18 μM we observed an increase in Sub-G1 population and reduction in S and G2/M populations (Fig. 3D). These finding were corroborated by mitotic index determination, therefore there was drastic reduction (62% and 76% for PIPE at 9 e 18 μM , respectively) in mitosis frequency. Concerning to clonogenic capacity, we observed that PIPE at 9 μM was capable of reducing colonies number in 63%, and no colonies were observed in samples treated with PIPE at 18 μM (Fig. 3B).

3.5. Expression profile of cyclin D1 and ERK

In next step, we sought to investigate molecular mechanism involved with antiproliferative activity of PIPE on A549 cells. For this purpose, and considering results previously obtained by flow cytometry, we evaluated the expression profile of cyclin D1 and extracellular signal-regulated kinase (ERK), a member of mitogen-activated protein kinase family (MAPK). According to immunoblot results (Fig. 3E and F), total ERK expression was not altered in consequence of PIPE treatment; by contrast, it reduced significantly cyclin D1 expression and ERK activation.

3.6. Apoptosis detection

Pro-apoptotic potential of PIPE on A549 cells was assessed initially by Annexin V/PI assay. After that, we verified the influence of PIPE on mitochondrial membrane depolarization using fluorescent probe JC-1. We observed an increase in frequency of cells positive for annexin V in treated cultures. Although, the percentage was significantly higher in cultures treated with PIPE at 18 μM (42%) in comparison to control samples (8%) (Fig. 4A). Further, we verified that pro-apoptotic activity of PIPE is related to intrinsic pathway activation. As shown in Fig. 4B, treated cells had lower $\Delta\psi_{\text{m}}$, once they exhibited more green

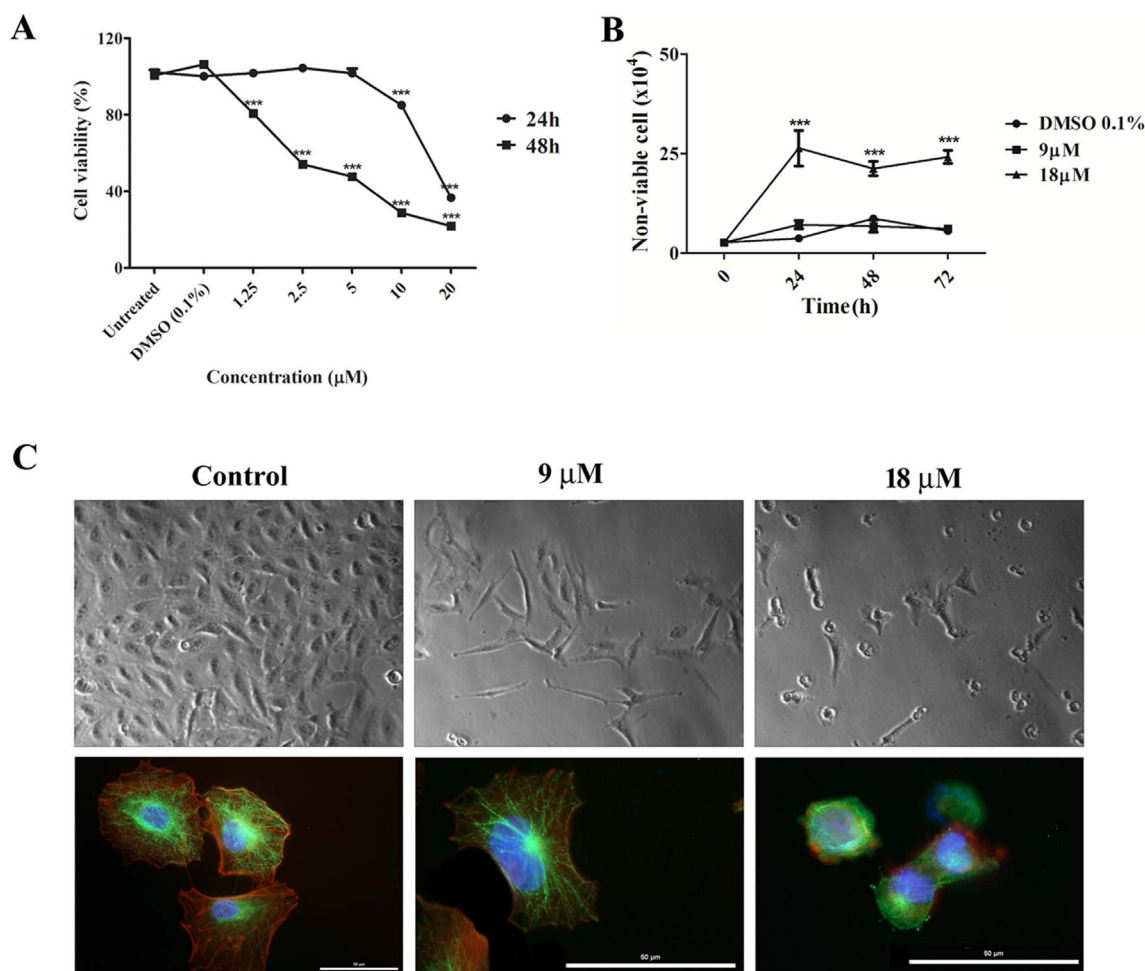


Fig. 2. (A) Cell viability determined by MTS assay after 24 h and 48 h of treatment with PIPE. (B) Non-viable cells population determined by trypan blue exclusion test at 24 h, 48 h and 72 h. (C) Phase contrast microscopy images (upper – 100 × magnification) showing morphology of A549 cells, and fluorescent images (lower – 400 × magnification) evidencing microfilaments (red) and microtubules (green) distribution pattern. Nuclei were stained with DAPI. ****p* < 0.001 using ANOVA followed by Tukey's post-test from 3 independent experiments. (For interpretation of the references to color in this figure legend, the reader is referred to the web version of this article.)

Table 3

IC₅₀ ± DP (μM) values determined from MTS assay.

	24 h	48 h
PIPE	17.99 ± 0.39	4.11 ± 0.27
Piperonylic acid	nd	nd
[RuCl ₂ (dppb)(bipy)]	nd	nd
Cisplatin ^a	61.84 ± 7.75	24.70 ± 4.78

nd = not determined; cell viability was not significantly altered in the used concentration range (0–100 μM).

^a Cisplatin was used as positive control.

fluorescence than control group. Quantitative analysis showed that the percentage of cells with lower of Δψ_m (higher ratio of green to red fluorescence) significantly increased when PIPE was used at 18 μM (34%) when compared to control samples (6%). We also verified increased frequency of positive cells for cleaved-caspase-3. In cultures treated at 9 μM and 18 μM we found, respectively, around 12% and 100% of positive cells for cleaved-caspase-3. Fig. 4C shows pattern of distribution observed for cleaved-caspase-3 on A549 cells.

4. Discussion

Ruthenium compounds have been considered a promising alternative to platinum-based drugs in cancer therapy, especially due to their selectivity (Barry and Sadler, 2013). Ruthenium complexes tend to

accumulate preferentially in neoplastic masses in comparison to normal tissue (Lazarević et al., 2017). Studies have been demonstrated that reduced toxicity of ruthenium compounds against healthy tissues may be related to different issues including the ability of the ruthenium to mimic iron in binding to many biological molecules such as transferrin and albumin (Pessoa and Tomaz, 2010; Palermo et al., 2016). In addition, solid tumor microenvironment generally displays reduction conditions (low pH and hypoxia), contributing for reduction of ruthenium(III) to ruthenium(II), the more active form of the ruthenium (Ravera et al., 2004; Gransbury et al., 2016). This reaction would provide not only a selective cytotoxicity, but also would contribute for overcoming resistance to chemotherapy and/or radiotherapy, commonly observed in hypoxic tumors (Sava and Bergamo, 2000).

Herein, we synthesized and characterized a novel ruthenium(II) complex [Ru(pipe)(dppb)(bipy)]PF₆, that displayed an important anti-proliferative and pro-apoptotic activity on A549 cells, which is derived from NSCLC.

Somatic mutations frequently observed in NSCLC include *TP53*, *EGFR* and *KRAS* (Lewandowska et al., 2012; Li et al., 2016a, b; Schneider et al., 2017). NSCLC patients with the *KRAS* mutation appear to be refractory to the majority of systemic therapies, and altered function of Ras protein lead to excessive activation of its downstream pathways including RAF/MEK/ERK signaling pathway (Sanders and Albitar, 2010). ERK1/2 overexpression is critical for sustaining proliferative behavior of tumor cells (Linardou et al., 2008; Rodenhuis et al., 1987; Lopez-Chavez et al., 2009). Thus, clinical research of new

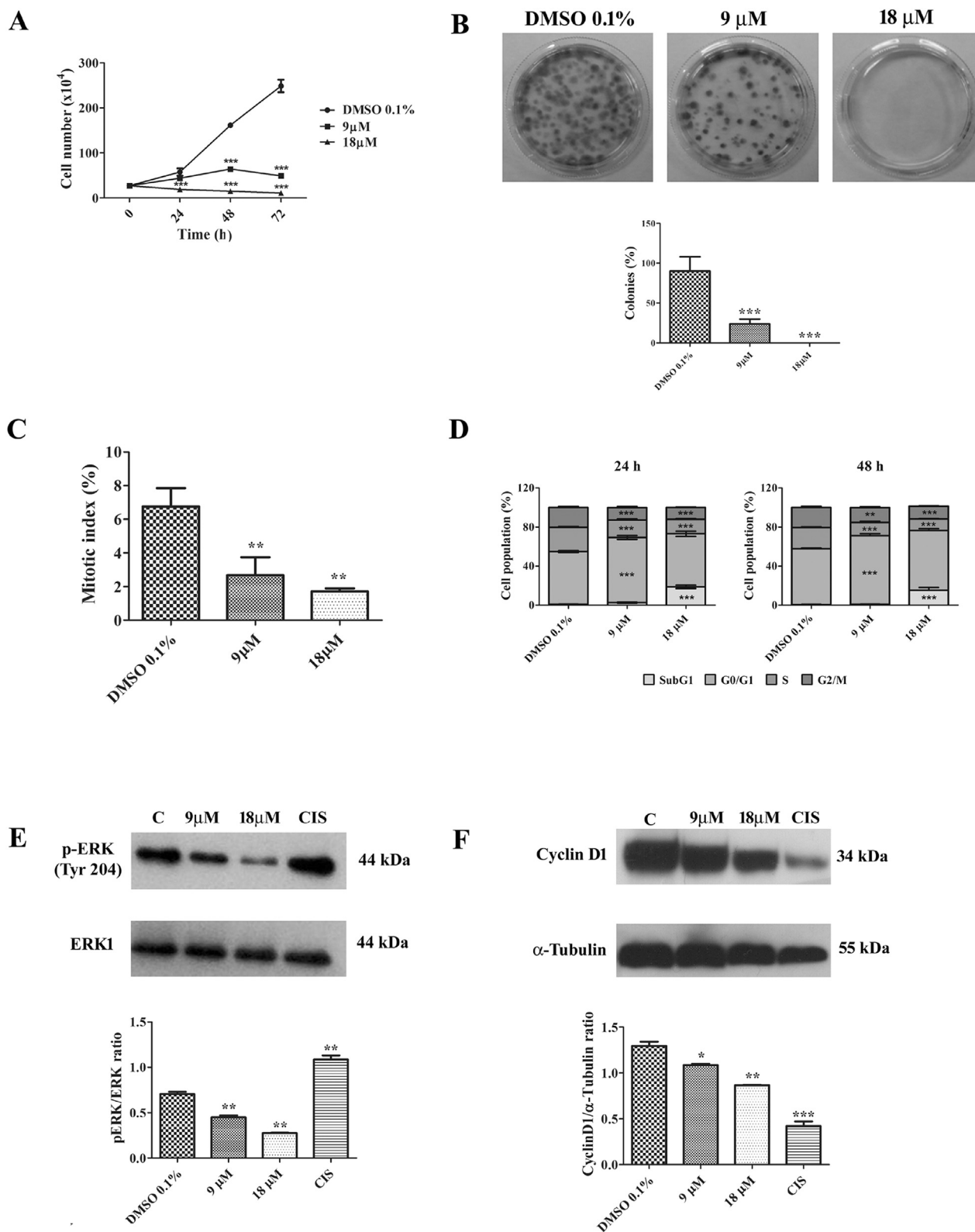


Fig. 3. (A) Growth curve of A549 cells. (B) Clonogenic capacity assay. (C) Mitotic index. (D) Cell cycle analysis. (E and F) Expression profile of Cyclin D1, ERK, and p-ERK. *p < 0.05, **p < 0.01 and ***p < 0.001 determined using ANOVA followed by Tukey's post-test from three independent experiments.

treatment strategies for NSCLC patients with *KRAS* mutations is urgently required.

We observed that PIPE was more active than cisplatin in reducing the viability of A549 cells, which harbor *KRAS* mutation but do not display alteration neither in *EGFR* nor in *TP53* (Furugaki et al., 2010;

Shao et al., 2011; Simonetti et al., 2010). Furthermore, cytotoxic potential of PIPE was higher against A549 than normal cells suggesting that the studied complex is selective for cancer cells. These findings corroborate with Lima et al. (2014) who demonstrated higher cytotoxicity of ruthenium complexes containing amino acids on sarcoma

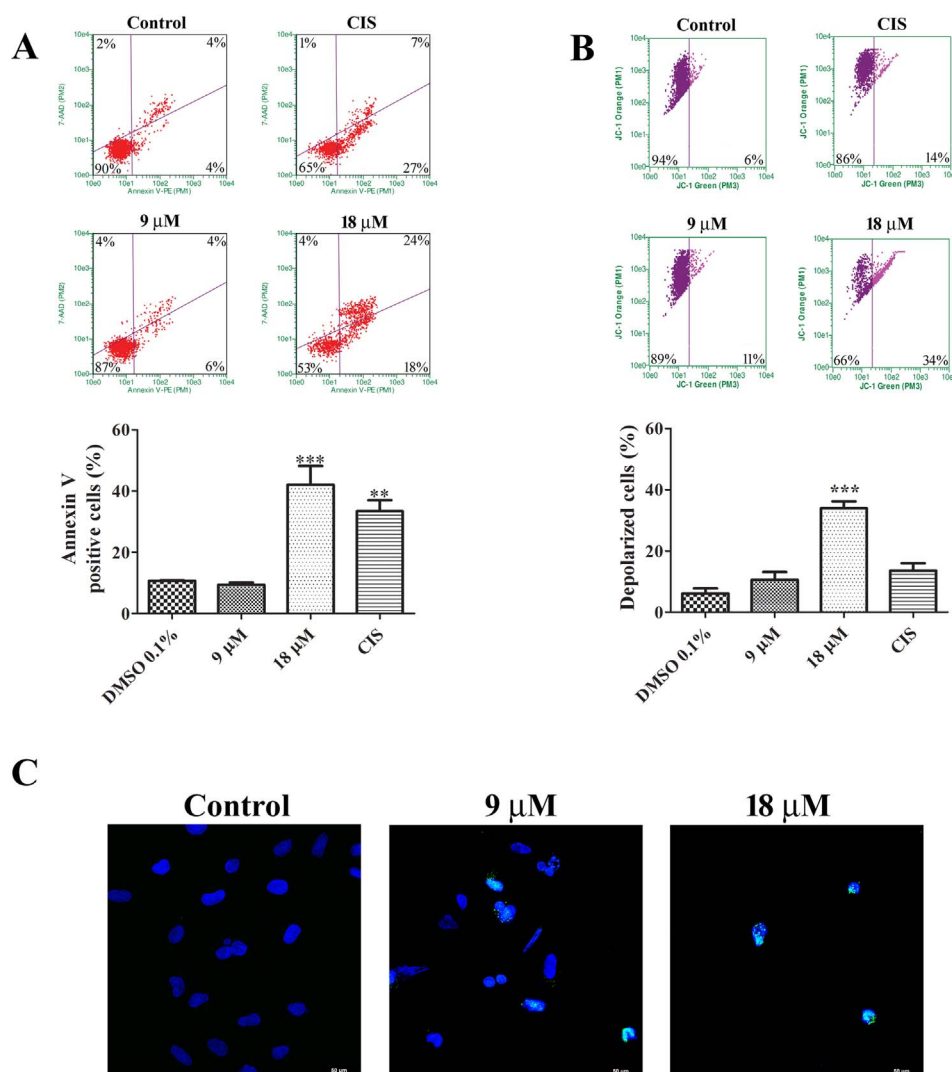


Fig. 4. (A) Annexin V-FITC/7-AAD assay. The lower left quadrants of each panel show the viable cells, which are negative for both 7-AAD and Annexin V-FITC. The upper left quadrants contain the non-viable, necrotic, negative for FITC-Annexin V binding and positive for 7-AAD cells. The lower right quadrants represent the cells in early apoptosis, that are Annexin V-FITC positive and 7-AAD negative. The upper right quadrants represent the cells in late apoptosis, positive for both Annexin V-FITC and 7-AAD. (B) Mitochondrial membrane potential using JC-1 as fluorescent probe. (C) Immunodetection for cleaved-caspase-3 (green). Nuclei were stained with DAPI. (For interpretation of the references to color in this figure legend, the reader is referred to the web version of this article).

cells (S180) than normal fibroblasts (L929), and [Iida et al. \(2016\)](#) who evidenced higher cytotoxic potential of ruthenium-arene complexes on breast cancer cells when compared to normal epithelial cells (MCF10A).

In the next step, we used different methodological approach to investigate deeply the biological mechanisms underlying PIPE activity on A549 cells, considering that the inhibition of cell viability by cytotoxic drugs can result from cycle cell arrest, apoptosis induction, or a combination of these two mechanisms ([Li et al., 2012](#); [Gaiddon et al., 2005](#)). For this purpose, further experiments were performed using PIPE at 18 μM and 9 μM, which correspond to IC_{50} and $IC_{50}/2$, determined at 24 h of treatment. We found that cytotoxic activity of PIPE is associated to its capacity of inhibiting cell proliferation and inducing apoptosis.

When sub-toxic concentration was used, PIPE had preferentially antiproliferative activity. We observed cell cycle arrest in G0/G1 transition, as demonstrated by increasing of G0/G1 cell population with concomitant reduction in S- and G2/M populations. Mitotic index was significantly reduced in samples treated with PIPE in comparison to control cultures corroborating with previous data obtained by flow cytometry. In addition, PIPE was effective in inhibiting clonogenic capacity of A549 cells demonstrating its negative influence on proliferative behavior of A549 even during prolonged period ([Ferreira-Silva et al., 2017](#); [Sales et al., 2015](#)). These findings are very interesting once sustained proliferative behavior of tumor cells is a critical event for tumor progression and metastasis ([Hanahan and Weinberg, 2011](#)).

The influence of ruthenium complexes on clonogenic capacity of tumor cells has been rarely explored, nevertheless it was reported by [Lima et al. \(2012\)](#) that *cis*-[RuCl₂(NH₃)₄]Cl inhibited the colony-formation ability of A549 cells. On the other hand, many studies have demonstrated that ruthenium complexes interfere on cell cycle progression; although the activity profile is variable according to the type of considered complex considered ([Lima et al., 2014](#); [De Lima et al., 2012](#); [Stepanenko et al., 2011](#); [Filak et al., 2010](#)). It has been reported that ruthenium(II)-arene complexes with paullone scaffold and ruthenium (II) complexed to glycine promote cell cycle arrest in G1/S transition ([Schmid et al., 2007](#); [Lima et al., 2014](#)). Accumulation of cells in the G0/G1 phase is often the result of cell cycle checkpoint activation ([Cassimere et al., 2016](#)). Studies have shown that some ruthenium compounds induce the arrest of cells in the G0/G1 phase through p53 activation in response to DNA damage, and an increase in the protein levels of p21, an inhibitor of the cell cycle that blocks CDK activity ([Chen et al., 2016](#); [Muthná et al., 2016](#)).

Cyclin D1 is a critical positive regulator of cell cycle, and it is responsible by activating CDK-cyclin complex of G1 phase. Different stimulus can activate gene transcription of cyclin D1 ([Qie and Diehl, 2016](#)); however, hyper-activation of the RAF/MEK/ERK signaling pathway is commonly observed in cancer cells that overexpression cyclin D ([Yadav et al., 2014](#)). Thereby, cyclin D1 and ERK expression profiles were assessed by immunoblot. The results showed that PIPE treatment significantly reduced cyclin D1 expression, but expression

levels of total-ERK were not altered. Interestingly, we detected significant reduction in ERK activation, as demonstrated by decreasing of phospho-ERK expression. Considering that cyclin D1 expression may be regulated by ERK, the cell cycle arrest induced by PIPE, at least in part, is associated to reduction of ERK activation. Although the influence of the ruthenium complexes on the activity of CDK-cyclin complexes has been investigated in cell-free system (Filak et al., 2010; Mühlgassner et al., 2012), up to now there is no data in the literature concerning inhibitory activity of ruthenium complexes on cyclins expression profile or Ras/MeK/Erk signaling pathway, especially considering the concentration range of PIPE used in the present study. Recently it was shown that a polypyridyl-ruthenium derived compound reduces ERK and pERK expression, nevertheless the authors did not investigate cyclins expression profile, and attributed the reduction of these proteins to pro-apoptotic activity of the studied compound (Deng et al., 2017).

In the last step, we investigated pro-apoptotic activity of PIPE on A549 cells considering previous data concerning morphological changes (cell shrinkage and loss cell-cell contact) and increased Sub-G1 cell population. We demonstrated that PIPE effectively induced apoptosis in A549 cells using specific markers of early (annexin V) and late (caspase 3) apoptosis. There was a significant increase in the frequency of positive cells for both annexin V and caspase 3. In addition, PIPE caused a loss of mitochondrial membrane potential demonstrating that apoptosis induced by PIPE was mediated, at least in part, by intrinsic pathway activation. Two main pathways of caspase activation have been described in mammalian cells (extrinsic and intrinsic), which result in final control of apoptosis. Extrinsic pathway is characterized by activating of death receptors, which are localized in plasma membrane, that in turn activate a cascade of events that mediate apoptosis process (Corazza et al., 2009). Intrinsic pathway, typically activated by intracellular stress signals, pro-apoptotic cell death factors belonging to the Bcl-2 family increase mitochondrial permeability and release cytochrome c, as well as other proteins from the intermembrane space of mitochondria; leading to apoptosome formation resulting in caspase-9 activation, which initiates a cascade of effector caspases including caspases-3, -6, and -7. In turn, the active caspase-3 triggers DNA fragmentation factor (Caspase-Activated DNase, CAD) and promotes DNA internucleosomal cleavage (Lopez and Tait, 2015). Many chemotherapeutic drugs induce apoptosis via intrinsic pathway by promoting DNA damage (Dewanjee et al., 2017; Zhong et al., 2013). It has been reported that the ruthenium complexes activate primary apoptosis by mitochondrial pathway (Lord et al., 2015; Huang et al., 2016; Yang et al., 2012). On the other hand, ruthenium complexes can activate the extrinsic apoptosis pathway (Li et al., 2012; Deng et al., 2015). Wan et al. (2017) demonstrated that ruthenium(II) polypyridyl complexes induce DNA damage due to their ability in increasing ROS in cells derived from carcinoma hepatocellular (BEL-7402 cells). Yang et al. (2012) demonstrated that ruthenium-methylimidazole complexes induced apoptosis in A549 cells through intrinsic mitochondrial pathway.

Considering that evasion to apoptosis is one of the central features of malignant progression as well as drug resistance, effective compounds in inducing apoptosis represent promising candidates as anti-neoplastic agent.

5. Conclusion

We synthesized and characterized a novel ruthenium(II)-piperonylic acid complex [Ru(pipe)(dppb)(bipy)]PF₆ and showed that it is a promising antitumor agent against non-small cell lung cancer due to its ability of inducing cell cycle arrest in G1/S transition and apoptosis by intrinsic pathway. We also demonstrated that the reduction of ERK activation and cyclin D1 expression are involved in the cycle arrest in G1/S transition induced by this ruthenium complex.

Conflicts of interest

The authors declare no conflicts of interest.

Transparency document

The <http://dx.doi.org/10.1016/j.tiv.2017.07.019> associated with this article can be found, in online version.

Acknowledgements

The authors are grateful to Brazilian Agencies CNPq (448723/2014-0 and 308162/2015-3), FAPEMIG (APQ02810-16, APQ-00273-14 and PPM-00533-16), CAPES (AUX PE – PNPd – 2347/2011), FAPESP, and FINEP for their financial support and to Marta Miyazawa for the language review. We also thank CNPq (A.C.D, F.T.M. and C.V), CAPES (G.A.F.S. and J.M.S.D), PIBICTI- FAPEMIG-UNIFAL-MG (M.M.O), PIBIC-CNPq-UNIFAL (G.Y.G) and PNPd-CAPES-PPGq-UNIFAL-MG (M.I.F.B) for the research fellowships. This study is a collaborative research project by members of the Rede Mineira de Química (RQ-MG), supported by FAPEMIG (Project: CEX-RED-00010-14).

References

- Allardyce, C.S., Dyson, P.J., 2001. Ruthenium in medicine: current clinical uses and future prospects. *Platin. Met. Rev.* 45, 62–69.
- Ang, C.W., Tweedle, E.M., Campbell, F., Rooney, P.S., 2011. Apical node metastasis independently predicts poor survival in Dukes C colorectal cancer. *Color. Dis.* 13 (5), 526–531.
- Antonarakis, E., Emadi, A., 2010. Ruthenium-based chemotherapeutics: are they ready for prime time? *Cancer Chemother. Pharmacol.* 66, 1–9.
- Barbosa, M.I.F., Correa, R.S., Pozzi, L.V., Lopes, E.O., Pavan, F.R., Leite, C.Q.F., Ellena, J., Machado, S.P., Poelhsitz, G.V., Batista, A.A., 2015. Ruthenium(II) complexes with hydroxypyridinecarboxylates: screening potential metallodrugs against *Mycobacterium tuberculosis*. *Polyhedron* 85, 376–382.
- Barry, N.P., Sadler, P.J., 2013. Challenges for metals in medicine: how nanotechnology may help to shape the future. *ACS Nano* 7 (7), 5654–5659.
- Bergamo, A., Sava, G., 2011. Ruthenium anticancer compounds: myths and realities of the emerging metal-based drugs. *Dalton Trans.* 40 (31), 7817–7823.
- Bergamo, A., Gaiddon, C., Schellens, J.H., Beijnen, J.H., Sava, G., 2012. Approaching tumour therapy beyond platinum drugs: status of the art and perspectives of ruthenium drug candidates. *J. Inorg. Biochem.* 106 (1), 90–99.
- Bezerra, D.P., Castro, F.O., Alves, A.P., Pessoa, C., Moraes, M.O., Silveira, E.R., Lima, M.A., Elmiro, F.J., Costa-Lotufo, L.V., 2006. In vivo growth-inhibition of Sarcoma 180 by piplartine and piperine, two alkaloid amides from Piper. *Braz. J. Med. Biol. Res.* 39 (6), 801–807.
- Brabc, V., Nováková, O., 2006. DNA binding mode of ruthenium complexes and relationship to tumor cell toxicity. *Drug Resist. Updat.* 9 (3), 111–122.
- Burla, M.C., Caliendo, R., Camalli, M., Carrozzini, B., Cascarano, G.L., De Caro, L., Giacobazzo, C., Polidori, G., Spagna, R., 2005. SIR2004: an improved tool for crystal structure determination and refinement. *J. Appl. Crystallogr.* 38, 381–388.
- Cassimere, E.K., Mauvais, C., Denicourt, C., 2016. p27Kip1 is required to mediate a G1 cell cycle arrest downstream of ATM following genotoxic stress. *PLoS One* 11 (9), e0162806.
- Chen, L.-m., Peng, F., Li, G.-d., Jie, X.-m., Cai, K., Cai, C., Zhong, Y., Zeng, H., Li, W., Zhang, Z., Chen, J.-c., 2016. The studies on the cytotoxicity in vitro, cellular uptake, cell cycle arrest and apoptosis-inducing properties of ruthenium methylimidazole complex [Ru(MeIm)₄(p-cpip)]₂·+. *J. Inorg. Biochem.* 156, 64–74.
- Corazza, N., Kassahn, D., Jakob, S., Badmann, A., Brunner, T., 2009. TRAIL-induced apoptosis: between tumor therapy and immunopathology. *Ann. N. Y. Acad. Sci.* 1171, 50–58.
- De Lima, A.P., Pereira, F.C., Vilanova-Costa, C.A., Soares, J.R., Pereira, L.C., Porto, H.K., Pavanin, L.A., Dos Santos, W.B., Silveira-Lacerda, E.P., 2012. Induction of cell cycle arrest and apoptosis by ruthenium complex cis-(dichloro)tetramineruthenium(III) chloride in human lung carcinoma cells A549. *Biol. Trace Elem. Res.* 147 (1–3), 8–15.
- Deng, Z., Yu, L., Cao, W., Zheng, W., Chen, T., 2015. Rational design of ruthenium complexes containing 2,6-bis(benzimidazolyl)pyridine derivatives with radiosensitization activity by enhancing p53 activation. *ChemMedChem* 10 (6), 991–998.
- Deng, Z., Gao, P., Yu, L., Ma, B., You, Y., Chan, L., Mei, C., Chen, T., 2017. Ruthenium complexes with phenylterpyridine derivatives target cell membrane and trigger death receptors-mediated apoptosis in cancer cells. *Biomaterials* 129, 111–126.
- Dewanjee, S., Joardar, S., Bhattacharjee, N., Dua, T.K., Das, S., Kalita, J., Manna, P., 2017. Edible leaf extract of *Ipomoea aquatica* Forssk. (Convolvulaceae) attenuates doxorubicin-induced liver injury via inhibiting oxidative impairment, MAPK activation and intrinsic pathway of apoptosis. *Food Chem. Toxicol.* 105, 322–336.
- Farrugia, L.J., 1997. ORTEP-3 for Windows - a version of ORTEP-III with a Graphical User Interface (GUI). *J. Appl. Crystallogr.* 30, 565.
- Ferreira-Silva, G.A., Lages, C.C., Sartorelli, P., Hasegawa, F.R., Soares, M.G., Ionta, M., 2017. Casearin D inhibits ERK phosphorylation and induces downregulation of cyclin D1 in HepG2 cells. *Toxicol. in Vitro* 38, 27–32.

- Filak, L.K., Mühlgassner, G., Jakupec, M.A., Heffeter, P., Berger, W., Arion, V.B., Keppler, B.K., 2010. Organometallic indolo[3,2-c]quinolines versus indolo[3,2-d]benzazepines: synthesis, structural and spectroscopic characterization, and biological efficacy. *J. Biol. Inorg. Chem.* 15 (6), 903–918.
- Flocke, L.S., Trondl, R., Jakupec, M.A., Keppler, B.K., 2016. Molecular mode of action of NKP-1339 - a clinically investigated ruthenium-based drug - involves ER- and ROS-related effects in colon carcinoma cell lines. *Investig. New Drugs* 34, 261–268.
- Franken, N.A., Rodermond, H.M., Stap, J., Haveman, J., van Bree, C., 2006. Clonogenic assay of cells in vitro. *Nat. Protoc.* 1 (5), 2315–2319.
- Furugaki, K., Iwai, T., Shirane, M., Kondoh, K., Moriya, Y., Mori, K., 2010. Schedule-dependent antitumor activity of the combination with erlotinib and docetaxel in human non-small cell lung cancer cells with EGFR mutation, KRAS mutation or both wild-type EGFR and KRAS. *Oncol. Rep.* 24, 1141–1146.
- Gaidon, C., Jeannequin, P., Bischoff, P., Pfeffer, M., Sirlin, C., Loeffler, J.P., 2005. Ruthenium (II)-derived organometallic compounds induce cytostatic and cytotoxic effects on mammalian cancer cell lines through p53-dependent and p53-independent mechanisms. *J. Pharmacol. Exp. Ther.* 315 (3), 1403–1411.
- Galanski, M., Arion, V.B., Jakupec, M.A., Keppler, B.K., 2003. Recent developments in the field of tumor-inhibiting metal complexes. *Curr. Pharm. Des.* 9, 2078–2089.
- Gransbury, G.K., Kappen, P., Glover, C.J., Hughes, J.N., Levina, A., Lay, P.A., Musgrave, I.F., Harris, H.H., 2016. Comparison of KP1019 and NAMI-A in tumour-mimetic environments. *Metallomics* 8 (8), 762–773.
- Hanahan, D., Weinberg, R.A., 2011. Hallmarks of cancer: the next generation. *Cell* 144 (5), 646–674.
- Hartering, C.G., Zorbas-Seiffried, S., Jakupec, M.A., Kynast, B., Zorbas, H., Keppler, B.K., 2006. From bench to bedside - pre-clinical and early clinical development of the anticancer agent indazolium trans-[tetrachlorobis(1H-indazole) ruthenate(III)] (KP1019 or FFC14A). *J. Inorg. Biochem.* 100, 891–904.
- Huang, S., Van Aken, O., Schwarzländer, M., Belt, K., Millar, A.H., 2016. The roles of mitochondrial reactive oxygen species in cellular signaling and stress response in plants. *Plant Physiol.* 171 (3), 1551–1559.
- Huxham, L.A., Cheu, E.L.S., Patrick, B.O., James, B.R., 2003. The synthesis, structural characterization, and in vitro anti-cancer activity of chloro(p-cymene) complexes of ruthenium(II) containing a disulfoligand. *Inorg. Chim. Acta* 352, 238–246.
- Iida, J., Bell-Loncella, E.T., Purazo, M.L., Lu, Y., Dorchak, J., Clancy, R., Slavik, J., Cutler, M.L., Shriver, C.D., 2016. Inhibition of cancer cell growth by ruthenium complexes. *J. Transl. Med.* 14 (48), 1–10.
- Komor, A.C., Barton, J.K., 2013. The path metal complexes to a DNA target. *Chem. Commun. (Camb.)* 49 (35), 3617–3630.
- Kostova, I., 2006. Platinum complexes as anticancer agents. *Recent Pat. Anticancer Drug Discov.* 1 (1), 1–22.
- Lai, L.H., Fu, Q.H., Liu, Y., Jiang, K., Guo, Q.M., Chen, Q.Y., Yan, B., Wang, Q.Q., Shen, J.G., 2012. Piperine suppresses tumor growth and metastasis in vitro and in vivo in a 4T1 murine breast cancer model. *Acta Pharmacol. Sin.* 33 (4), 523–530.
- Lazarević, T., Rilak, A., Bugarčić, Ž.D., 2017. Platinum, palladium, gold and ruthenium complexes as anticancer agents: current clinical uses, cytotoxicity studies and future perspectives. *Eur. J. Med. Chem.* S0223–5234 (17), 30262–30263.
- Lewandowska, M.A., Józwicki, W., Starzyński, J., 2012. Analysis of EGFR mutation frequency and coexistence of KRAS and EGFR mutations using RT-PCR in lung adenocarcinoma: may a clinical and pathological model of a patient's qualification for targeted therapy have an impact on time to obtain genetic results? *Kardiochir Torakochir Pol.* 9, 443–451.
- Li, L., Wong, Y.S., Chen, T., Fan, C., Zheng, W., 2012. Ruthenium complexes containing bis-benzimidazole derivatives as a new class of apoptosis inducers. *Dalton Trans.* 41 (4), 1138–1141.
- Li, J., Wang, S., Su, Z.-F., Yuan, Y., 2016a. Synergistic effects of sorafenib in combination with gemcitabine or pemetrexed in lung cancer cell lines with K-ras mutations. *Contemp. Oncol. (Pozn.)* 20 (1), 33–38.
- Li, W., Zhang, Z., Guo, L., Qiu, T., Ling, Y., Cao, J., Guo, H., Zhao, H., Li, L., Ying, J., 2016b. Assessment of cytology based molecular analysis to guide targeted therapy in advanced non-small-cell lung cancer. *Oncotarget* 7 (7), 8332–8340 (Feb 16).
- Lima, A.L., Pereira, F.C., Almeida, M.A.P., Mello, F.M.S., Pires, W.C., Pinto, T.M., Delella, F.K., Felisbino, S.L., Moreno, V., Batista, A.A., Silveira-Lacerda, E.P., 2014. Cytotoxicity and apoptotic mechanism of ruthenium(II) amino acid complexes in sarcoma-180 tumor cells. *PLoS One* 9 (10), 1–11.
- Linardou, H., Dahabreh, I.J., Kanakoupiti, D., 2008. Assessment of somatic k-Ras mutations as a mechanism associated with resistance to EGFR-targeted agents: a systematic review and meta-analysis of studies in advanced non-small-cell lung cancer and metastatic colorectal cancer. *Lancet Oncol.* 9, 962–972.
- Lopez, J., Tait, S.W., 2015. Mitochondrial apoptosis: killing cancer using the enemy within. *Br. J. Cancer* 112 (6), 957–962.
- Lopez-Chavez, A., Carter, C.A., Giaccone, G., 2009. The role of KRAS mutations in resistance to EGFR inhibition in the treatment of cancer. *Curr. Opin. Investig. Drugs* 10, 1305–1314.
- Lord, R.M., Hebden, A.J., Pask, C.M., Henderson, I.R., Allison, S.J., Shepherd, S.L., Phillips, R.M., McGowan, P.C., 2015. Hypoxia-sensitive metal β -ketoiminato complexes showing induced single-strand DNA breaks and cancer cell death by apoptosis. *J. Med. Chem.* 58 (12), 4940–4953.
- Macrae, C.F., Bruno, I.J., Chisholm, J.A., Edgington, P.R., McCabe, P., Pidcock, E., Monge, L.R., Taylor, R., van de Streek, J., Wood, P.A., 2008. Mercury CSD 2.0 - new features for the visualization and investigation of crystal structures. *J. Appl. Crystallogr.* 41, 466–470.
- Mühlgassner, G., Bartel, C., Schmid, W.F., Jakupec, M.A., Arion, V.B., Keppler, B.K., 2012. Biological activity of ruthenium and osmium arene complexes with modified pailones in human cancer cells. *J. Inorg. Biochem.* 116, 180–187.
- Muthná, D., Tomšík, P., Havelek, R., Köhlerová, R., Kasilingam, V., Čermáková, E., Stíbal, D., Řezáčová, M., Süß-Fink, G., 2016. In-vitro and in-vivo evaluation of the anticancer activity of diruthenium-2, a new trithiolato arene ruthenium complex $[\eta^6\text{-p-MeC}_6\text{H}_4\text{Pri}]_2\text{Ru}_2(\mu\text{-S-p-C}_6\text{H}_4\text{OH})_3\text{Cl}$. *Anti-Cancer Drugs* 27 (7), 643–650.
- Palermo, G., Magistrato, A., Riedel, T., von Erlach, T., Davey, C.A., Dyson, P.J., Rothslerberger, U., 2016. Fighting cancer with transition metal complexes: from naked DNA to protein and chromatin targeting strategies. *ChemMedChem* 11 (12), 1199–1210.
- Pereira, R.M., Ferreira-Silva, G.Á., Pivatto, M., Santos, L.Á., Bolzani, V.S., Chagas de Paula, D.A., Oliveira, J.C., Viegas Júnior, C., Ionta, M., 2016. Alkaloids derived from flowers of *Senna spectabilis*, (–)-cassine and (–)-spectaline, have antiproliferative activity on HepG2 cells for inducing cell cycle arrest in G1/S transition through ERK inactivation and downregulation of cyclin D1 expression. *Toxicol. in Vitro* 31, 86–92.
- Pessoa, J.C., Tomaz, I., 2010. Transport of therapeutic vanadium and ruthenium complexes by blood plasma components. *Curr. Med. Chem.* 17 (31), 3701–3738.
- Qie, S., Diehl, J.A., 2016. Cyclin D1, cancer progression, and opportunities in cancer treatment. *J. Mol. Med. (Berl.)* 294 (12), 1313–1326.
- Queiroz, S.L., Batista, A.A., Oliva, G., Gambardella, M.T.P., Santos, R.H.A., MacFarlane, K.S., Rettig, S.J., James, B.R., 1998. The reactivity of five-coordinate Ru(II) (1,4-bis(diphenylphosphino)butane) complexes with the N-donor ligands: ammonia, pyridine, 4-substituted pyridines, 2,2'-bipyridine, bis(o-pyridyl)amine, 1,10-phenanthroline, 4,7-diphenylphenanthroline and ethylenediamine. *Inorg. Chim. Acta* 267, 209.
- Ravera, M., Baracco, S., Cassino, C., Zanella, P., Osella, D., 2004. Appraisal of the redox behaviour of the antimetastatic ruthenium(III) complex $[\text{ImH}][\text{RuCl}(\text{4})(\text{DMSO})(\text{Im})]$, NAMI-A. *Dalton Trans.* 7 (15), 2347–2351.
- Reck, M., Krzakowski, M., Chmielowska, E., Sebastian, M., Hadler, D., Fox, T., Wang, Q., Greenberg, J., Beckman, R.A., von Pawel, J., 2013. A randomized, double-blind, placebo-controlled phase 2 study of tigatuzumab (CS-1008) in combination with carboplatin/paclitaxel in patients with chemotherapy-naïve metastatic/unresectable non-small cell lung cancer. *Lung Cancer* 82 (3), 441–448.
- Rodenhuis, S., van de Wetering, M.L., Mooi, W.J., 1987. Mutational activation of the K-ras oncogene. A possible pathogenetic factor in adenocarcinoma of the lung. *N. Engl. J. Med.* 317, 929–935.
- Sales, L., Pezuk, J.A., Borges, K.S., Brascoso, M.S., Scrideli, C.A., Tone, L.G., dos Santos, M.H., Ionta, M., de Oliveira, J.C., 2015. Anticancer activity of 7-epiclusianone, a benzophenone from *Garcinia brasiliensis*, in glioblastoma. *BMC Complement. Altern. Med.* 15, 393.
- Sanders, H.R., Albitar, M., 2010. Somatic mutations of signaling genes in non-small-cell lung cancer. *Cancer Genet. Cytogenet.* 203, 7–15.
- Sava, G., Bergamo, A., 2000. Ruthenium based compounds and tumor growth control. *Int. J. Oncol.* 17, 353–365 (review).
- Sava, G., Pacor, S., Zorzet, S., Alessio, E., Mestroni, G., 1989. Antitumour properties of dimethylsulphoxide ruthenium (II) complexes in the Lewis lung carcinoma system. *Pharmacol. Res.* 21 (5), 617–628.
- Schmid, W.F., John, R.O., Mühlgassner, G., Heffeter, P., Jakupec, M.A., Galanski, M., Berger, W., Arion, V.B., Keppler, B.K., 2007. Metal-based pailones as putative CDK inhibitors for antitumor chemotherapy. *J. Med. Chem.* 50, 6343–6355.
- Schneider, G., Schmidt-Supprin, M., Rad, R., Saur, D., 2017. Tissue-specific tumorigenesis: context matters. *Nat. Rev.* 17, 239.
- Scolaro, C., Bergamo, A., Brescacin, L., Delfino, R., Cocchiello, M., Laurency, G., Geldbach, T.J., Sava, G., Dyson, P.J., 2005. In vitro and in vivo evaluation of ruthenium(II)-arene PTA complexes. *J. Med. Chem.* 48, 4161–4171.
- Shao, C., Lu, C., Chen, L., Koty, P.P., Cobos, E., Gao, W., 2011. p53-Dependent anticancer effects of leptomycin B on lung adenocarcinoma. *Cancer Chemother. Pharmacol.* 67 (6), 1369–1380.
- Sheldrick, G.M., 2008. A short history of SHELX. *Acta Crystallogr. Sect. A* 64, 112–122.
- Si, Y.-X., Ji, S., Fanga, N.-Y., Wang, W., Yang, J.-M., Qiana, G.-Y., Parka, Y.-D., Lee, J., Yina, S.-J., 2013. Effects of piperonylic acid on tyrosinase: mixed-type inhibition kinetics and computational simulations. *Process Biochem.* 48 (11), 1706–1714.
- Simonetti, S., Molina, M.A., Queral, C., de Aguirre, I., Mayo, C., Bertran-Alamillo, J., Sanchez, J.J., Gonzalez-Larriba, J.L., Jimenez, U., Isla, D., Moran, T., Viteri, S., Camps, C., Garcia-Campelo, R., Massuti, B., Benlloch, S., Ramon y Cajal, S., Taron, M., Rosell, R., 2010. Detection of EGFR mutations with mutation-specific antibodies in stage IV non-small-cell lung cancer. *J. Transl. Med.* 18 (8), 135.
- Stepanenko, I.N., Casini, A., Edefe, F., Novak, M.S., Arion, V.B., Dyson, P.J., Jakupec, M.A., Keppler, B.K., 2011. Conjugation of organoruthenium(II) 3-(1H-benzimidazol-2-yl)pyrazolo[3,4-b]pyridines and indolo[3,2-d]benzazepines to recombinant human serum albumin: a strategy to enhance cytotoxicity in cancer cells. *Inorg. Chem.* 50, 12669–12679.
- Sunila, E.S., Kuttan, G., 2004. Immunomodulatory and antitumor activity of *Piper longum* Linn. and piperine. *J. Ethnopharmacol.* 90 (2–3), 339–346.
- Wan, D., Lai, S.H., Zeng, C.C., Zhang, C., Tang, B., Liu, Y.J., 2017. Ruthenium(II) polypyridyl complexes: synthesis, characterization and anticancer activity studies on BEL-7402 cells. *J. Inorg. Biochem.* 173, 1.
- Yadav, V., Burke, T.B., Huber, L., 2014. Upregulation resistance resulting from MAPK reactivation and cyclin D1 upregulation. *Mol. Cancer Ther.* 13, 2253–2263.
- Yang, X., Chen, L., Liu, Y., Yang, Y., Chen, T., Zheng, W., Liu, J., He, Q.-Y., 2012. Ruthenium methylimidazole complexes induced apoptosis in lung cancer A549 cells through intrinsic mitochondrial pathway. *Biochimie* 94, 345–353.
- Zarai, Z., Boujelbene, E., Salem, N.B., Gargouri, Y., Sayari, A., 2013. Antioxidant and antimicrobial activities of various solvent extracts, piperine and piperic acid from *Piper nigrum*. *LWT-Food Sci. Technol.* 50, 634–641.
- Zhong, Y.J., Liu, S.P., Firestone, R.A., Hong, Y.P., Li, Y., 2013. Anticancer effects of Ac-Phe-Lys-PABC-doxorubicin via mitochondria-centered apoptosis involving reactive oxidative stress and the ERK1/2 signaling pathway in MGC-803 cells. *Oncol. Rep.* 30 (4), 1681–1686.